U.S. DEPARTMENT OF THE INTERIOR

U.S. GEOLOGICAL SURVEY

The July 1992 Seismic Calibration Experiment along the Landers, California Earthquake Rupture

by

Donna Eberhart-Phillips and Jim Mori

Open-File Report 94-590

U. S. Geological Survey
525 South Wilson Ave.
Pasadena, CA 91106

1994

ABSTRACT

A seismic experiment to measure the crustal velocity structure was conducted in July 1992 along a 110 km profile parallel to the fault rupture of the Landers earthquake (M_W 7.3), with 2 calibration shots and 41 temporary recording sites. The data recorded on the portable instruments from the explosions and 42 earthquakes were combined with arrival times from the Southern California Seismic Network to obtain a three-dimensional P-wave (Vp) velocity model and estimates of the the P- to S-wave velocity ratio (Vp/Vs). The results show velocity variations along the fault that may be related to the material properties that controlled the rupture of the 1992 Landers earthquake. There is a prominent high velocity zone near the area of greatest slip in the central portion of the fault rupture and lower velocities near the northern and southern ends of the fault. The Vp/Vs ratios are greater at shallow depths less than 5 km. Relocations of earthquakes using the derived velocity model tend to have deeper hypocenters than the locations from the permanent network. The relocated depth of the Landers mainshock was estimated to be 3.0 ±1.0 km.

INTRODUCTION

The M_w 7.3 June 28, 1992 Landers earthquake and aftershock sequence occurred in a sparsely instrumented portion of the Southern California Seismic Network (SCSN). The mainshock hypocenter, as determined with the SCSN data, is relatively shallow and poorly constrained. In order to determine the local velocity structure and obtain a better estimate of the mainshock depth, the USGS conducted a seismic experiment using two explosive sources with known hypocenters along the fault rupture. One shot was located near the mainshock epicenter and the second shot was located 40 km farther north, near the southern end of the Camp Rock Fault section of the rupture (Table 1). We deployed 42 three-component data recorders in a 110 km long profile, approximately paralleling the trend of the rupture (Figure 1). The instruments recorded 160 earthquakes as well as the shots.

Preliminary modelling has been previously done using the arrival times of the calibration shots at the SCSN stations to obtain a one-dimensional velocity model and station corrections appropriate for relocating earthquakes in the Landers area (Hauksson, et al., 1993). Variation in the resulting station corrections shows that the crust is heterogeneous, thus three-dimensional modelling should improve the velocity model and hypocentral locations. In this report we present a three-dimensional velocity model developed using the shots and earthquakes recorded during the calibration experiment.

Shot	Date	Hr Min Sec	Latitude	Longitude	Elevation
1	7/17/92	6 0 0.00	34° 12.90'	116° 25.15'	1150 m
2	7/17/92	6 3 0.00	34° 33.54'	116° 34.33'	1020 m

Table 1. Origin times and locations of calibration explosions.

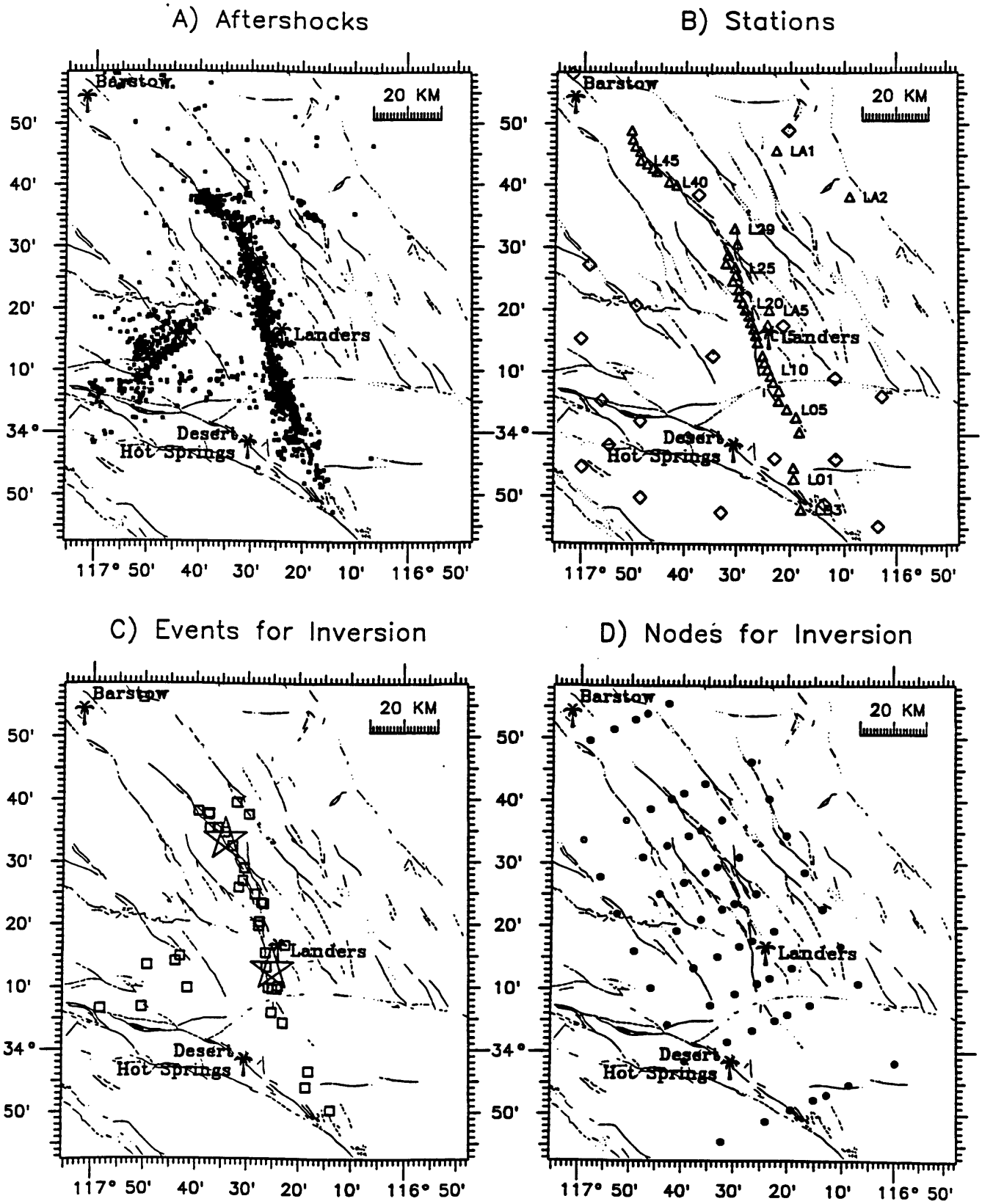

Figure 1. Maps for the region of the calibration experiment along the 1992 Landers rupture: (A) aftershock distribution, (B) station distribution, (C) events used in inversion, and (D) node locations used in the inversion. On the station map triangles are the temporary sites and diamonds are permanent stations of the SCSN. Additional SCSN stations were used that are outside of this map area. On the event map, the large stars show locations of the calibration shots and squares show the earthquakes used for the inversion.

DATA

The temporary stations consisted of Reftek 72A-06 data recorders with Mark Products L-28 LBH 3-component geophones that had a natural frequency of 4.5 hz.. Three high-gain and three low-gain channels were recorded at each of the sites. In addition to the calibrations shots, we gathered data from the ongoing aftershock activity by recording continuously in 5 minute segments for 1.2 days. The digital data were sampled at 100 hz, except for site LU3 which was set at 250 hz.

The experiment produced over 24 hours of continuous data from each station that was played back into PASSCAL format *seg-y* files. From the continuous data we extracted the two calibration shots and all M≥2 earthquakes. In addition, we ran the SEGYTRIGGER program (Aaron Martin, UCSB, written communication, 1992) over the continuous records from each station and saved all the event triggers. The PASSCAL program SEGYMERGE was used to extract designated time windows of data.

We associated the data files from the individual stations into events using the PASSCAL program REAP. The *seg-y* files were converted to *ah* format and combined event files. We examined the data in each of these event files and deleted most of the extraneous traces that were associated by REAP. The complete list of *ah* event files is shown in Table 4. Figure 2 shows record sections for the first calibration shot and an earthquake on July 17, 1991 at 0357. These data are available from the Southern California Earthquake Center (SCEC) data center.

TIMING CORRECTIONS

The standard procedure to obtain accurate time with the Reftek instruments is to record timing pulses to data stream 08. Ideally this was done at the time the instrument was first deployed and again when the instrument stopped recording. The offset and drift can then be calculated and clock corrections applied to all trace files. This procedure was

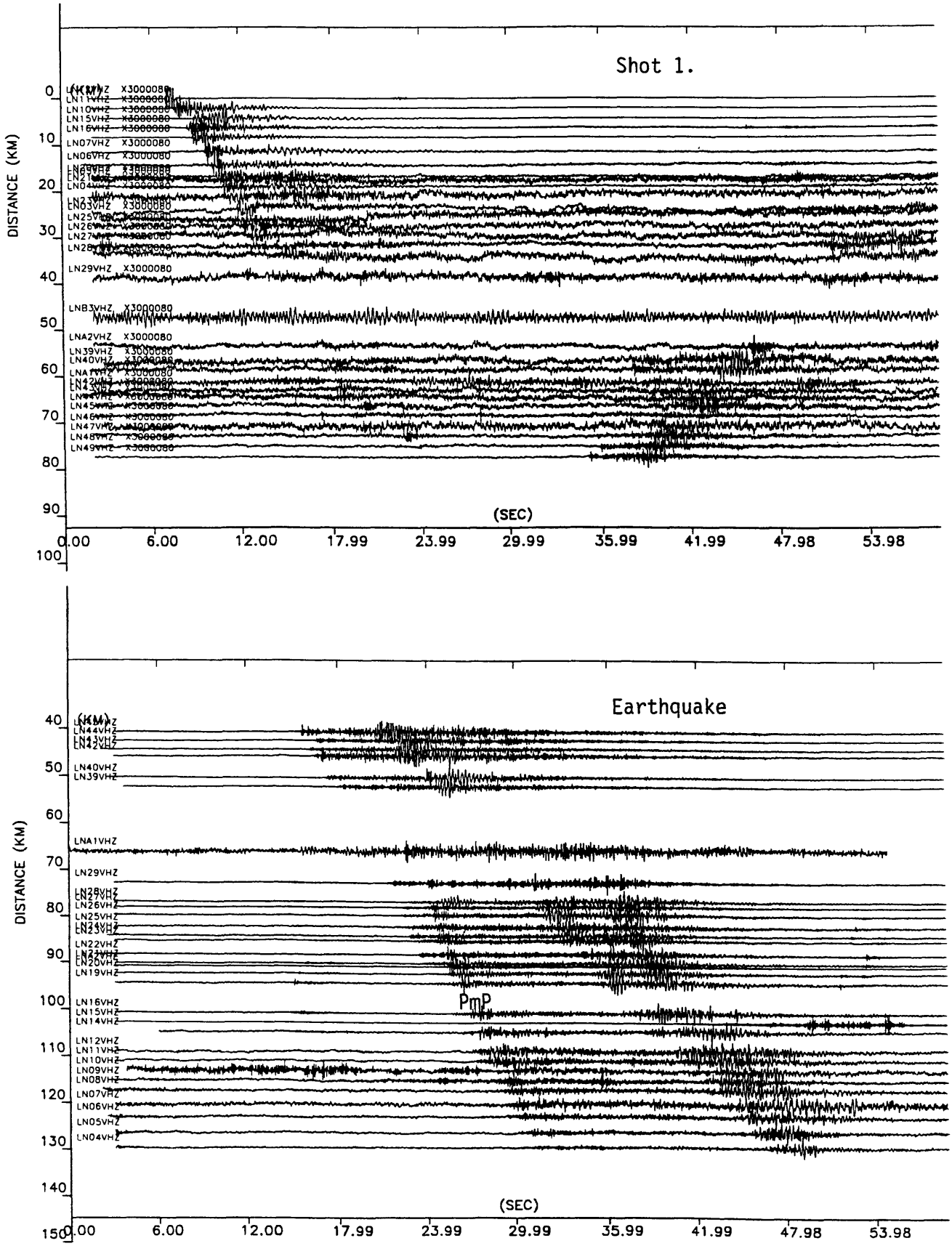

Figure 2. Record sections of the first calibration shot (top) and an earthquake on July 17 at 0357 (bottom) recorded on the portable stations. A clear Moho reflection (PmP) can be seen on the earthquake data between 24 and 30 sec.

carried out for instruments that have recorded values of the offset and drift, as shown in Table 3. Many stations only had an offset recorded at either the beginning or the end of the deployment but not both. In those cases, the offsets were used with zero drift. Laboratory tests of the recorders showed that the drift was negligible over the short time period (~24 hours) of deployment. Tested drifts that were available are shown in Table 3.

For some instruments more effort was necessary to obtain an accurate timing correction. We looked in detail at the event files for several earthquakes and compared the expected arrival times to the apparent arrival times for stations that had problematic offsets. In some cases multiple pulses were recorded to data stream 08, some of which were random spurious pulses. Using the expected arrival time of the recorded P wave, it was possible to identify which pulses were the correct timing pulses.

Timing corrections are more uncertain for stations that have only estimated offsets listed in Table 3. In some cases the instrument time was off by more than 60 sec. For these stations, the calculated offset was wrong, but it could be combined with an integer number of minutes to get a useful estimated offset. In other cases there were no recorded timing pulses to data stream 08. For these data we could estimate the offset only by evaluating several earthquake records for each station. It is worth noting that if we had programmed only to capture the shots and not recorded continuously, we would have completely missed the desired traces at these stations with very large offsets.

The recorded and estimated offsets listed in Table 3 were used to correct the data. These time corrections have been made to the data in the *ah* event files. Arrival-time data from stations with only estimated offsets were included in the velocity inversions discussed later in this report. To accomodate uncertainties in the timing of these stations, station correction parameters were included in the inversion. The calculated station corrections are included in Table 3. These station corrections are fairly stable: the calculated station corrections for individual stations differed by less than 0.07 s among the 1-D and various

3-D inversions. The calculated station corrections listed in Table 3 were not applied to the *ah* format event data files.

THREE-DIMENSIONAL VELOCITY STRUCTURE

Since we recorded both earthquakes and the calibration shots on three-component stations, we used P and S-P arrival times from both the passive and active sources in a simultaneous inversion for hypocenters, three-dimensional P-wave velocity (Vp), and three-dimensional P- to S-wave velocity ratio (Vp/Vs) along the Landers rupture. We timed 42 spatially distributed earthquakes (Figure 1) using the program EPICK (Bruce Julian, written communication, 1992). Arrival-times from the Southern California Seismic Network (SCSN) were also included for the same events. The earthquakes ranged in magnitude from 1.7 to 3.8 and had 14 to 98 observations each. The energy from the shots coupled into the ground rather poorly and did not propagate very efficiently. We carefully timed the arrivals, although the shots were observed only weakly beyond 15 km. SP1, near the mainshock epicenter, had good arrivals at 19 SCSN stations and 15 of the temporary sites. SP2, the northern shot, had good arrivals at 28 SCSN stations and 19 temporary sites.

The simultaneous inversion method used in this study is described by Thurber (1983), Thurber (1993) and Eberhart-Phillips (1993). The initial one-dimensional model (Figure 3) was obtained with this data set using the VELEST program (Urs Kradolfer and Edi Kissling, written communication, 1992). It is similar to the one-dimensional model derived by Hauksson et al. (1993) using solely SCSN data (Figure 3). In the upper crust, the two models are similar but our version has more layers and it can accomodate more of a velocity gradient.

The three-dimensional grid of node points used for the inverion is shown in Figure 1. The final velocity model was obtained using a series of inversions with successively finer grids. As shown in Figure 4, the resulting solution is presented by a series of Vp

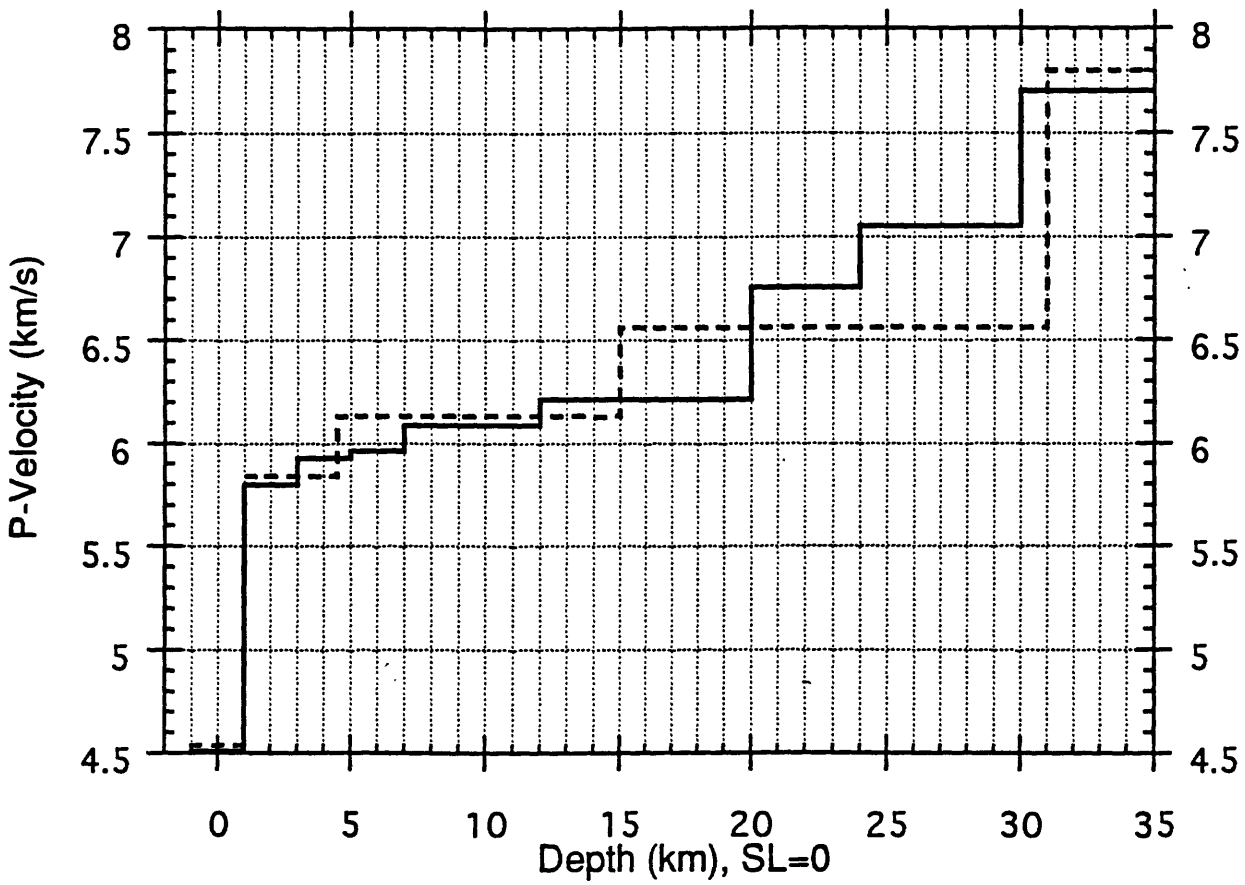

Figure 3. One-dimensional P-wave velocity model from inversion of data presented in this study (solid line) compared with model from inversion of only SCSN data (dotted line) by Hauksson et al., (1993).

cross-sections oriented normal to the trend of the Landers rupture (Figure 5), also Vp and Vp/Vs cross-sections that parallel the Landers rupture (Figure 6 and 7).

Overall, the three-dimensional model shows fairly uniform velocities with less heterogeneity than found in some other areas that have been studied along the San Andreas fault (Michael and Eberhart-Phillips, 1991; Eberhart-Phillips and Michael, 1993). The fault that ruptured in the Landers M_W 7.3 earthquake (Sieh et al., 1993) is not clearly expressed in the three-dimensional velocity structure. However, there are some interesting velocity variations that may help explain the character of the Landers rupture.

The sections nearest to the mainshock epicenter (Figure 5, sections F and G), which contain the Johnson Valley fault segment, suggest that the fault zone can be imaged. These sections show a slight vertical low-velocity zone (LVZ) in the shallow (<2 km) region close to the fault trace, which is located in the middle of the cross sections at the distance of 30 km. A vertical LVZ has been inferred here by Li et al (1994) based on fault zone trapped waves. Below 4 km depth the fault is defined by a horizontal velocity gradient with higher velocity on the east side.

The block south of the Landers rupture and south of the Pinto Mountain fault has a velocity image which is distinctive in having higher velocity material west of the fault rupture below 8 km depth (Figure 5, section H). The southernmost cross-section (Figure 5, section I) shows a well developed low-velocity zone across the San Andreas fault zone at depths less than 10 km.

The velocity image for the region north of the Johnson Valley segment shows the largest velocity variation. Along the Landers and Homestead Valley segments, the velocity is relatively uniform (Figure 5, section E). However at the juncture of the Homestead Valley and Emerson segments, where the bend in the aftershock trend and surface rupture is best defined, there is a pronounced high-velocity body east of the fault rupture (Figure 5, section D). The high-velocity body is located at a relatively shallow depth between the Emerson fault segment of the Landers rupture and the Calico fault to

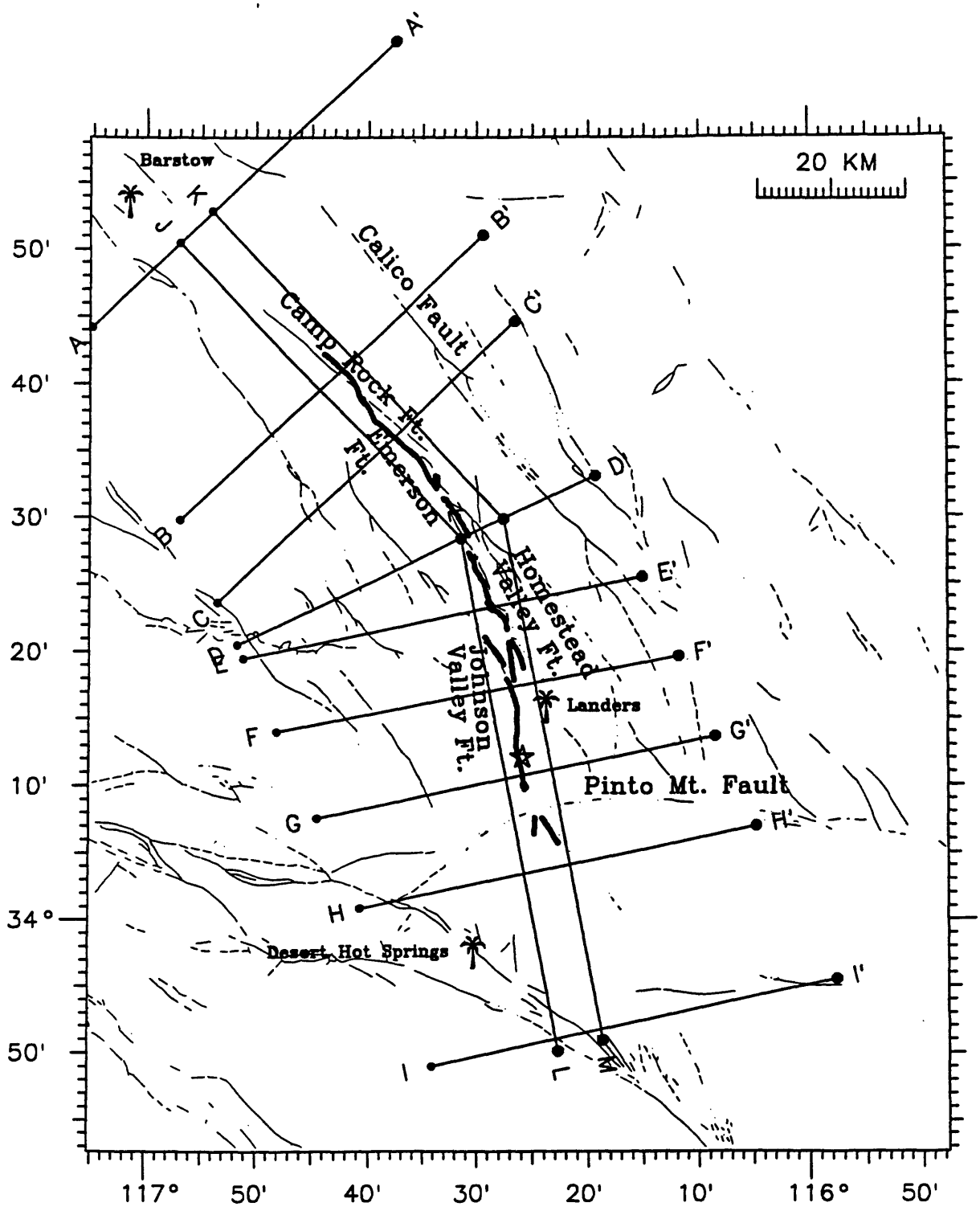

Figure 4. Map showing the orientations of the cross sections plotted in Figures 5, 6, and 7 along with the surface rupture (dark lines).

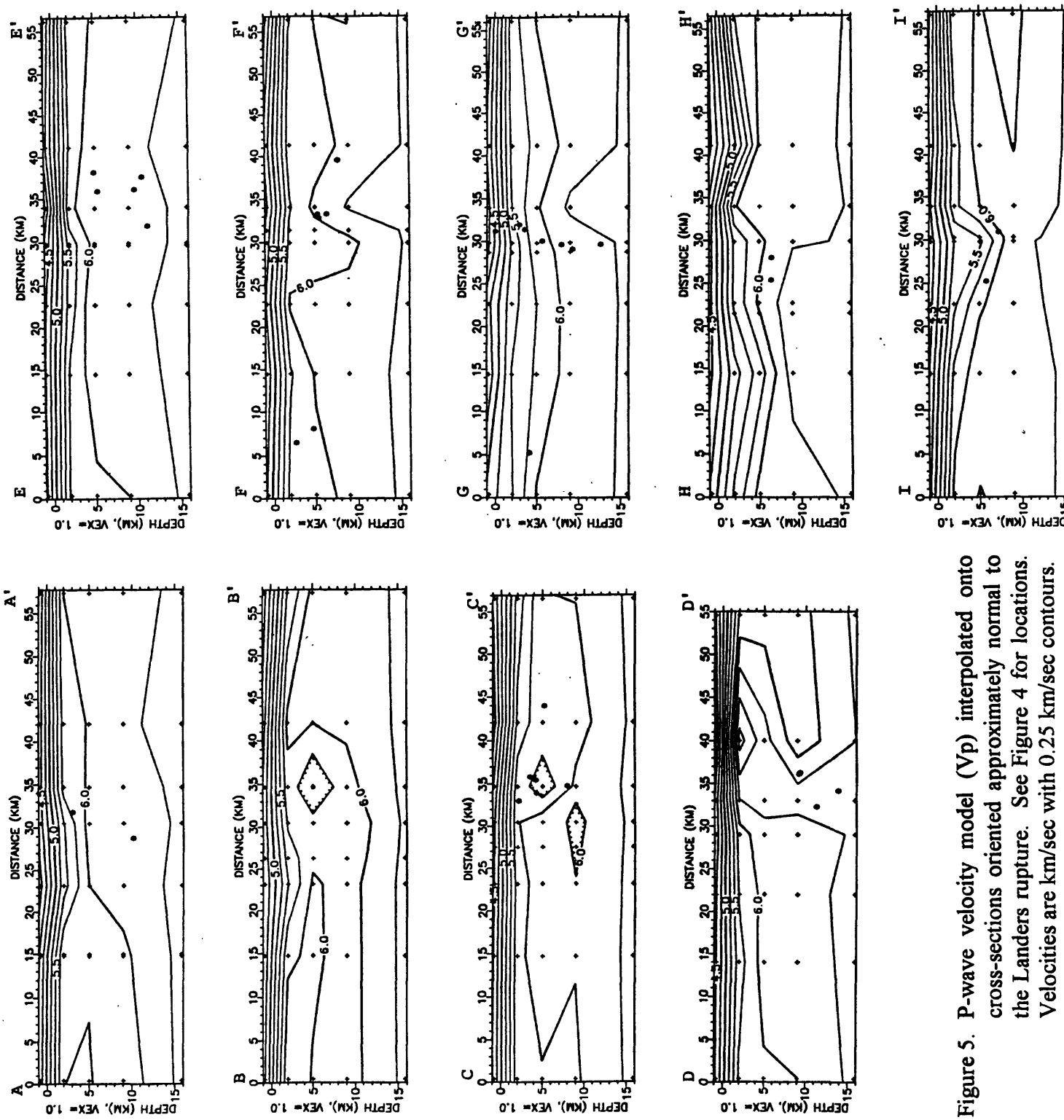

Figure 5. P-wave velocity model (Vp) interpolated onto cross-sections oriented approximately normal to the Landers rupture. See Figure 4 for locations. Velocities are km/sec with 0.25 km/sec contours.

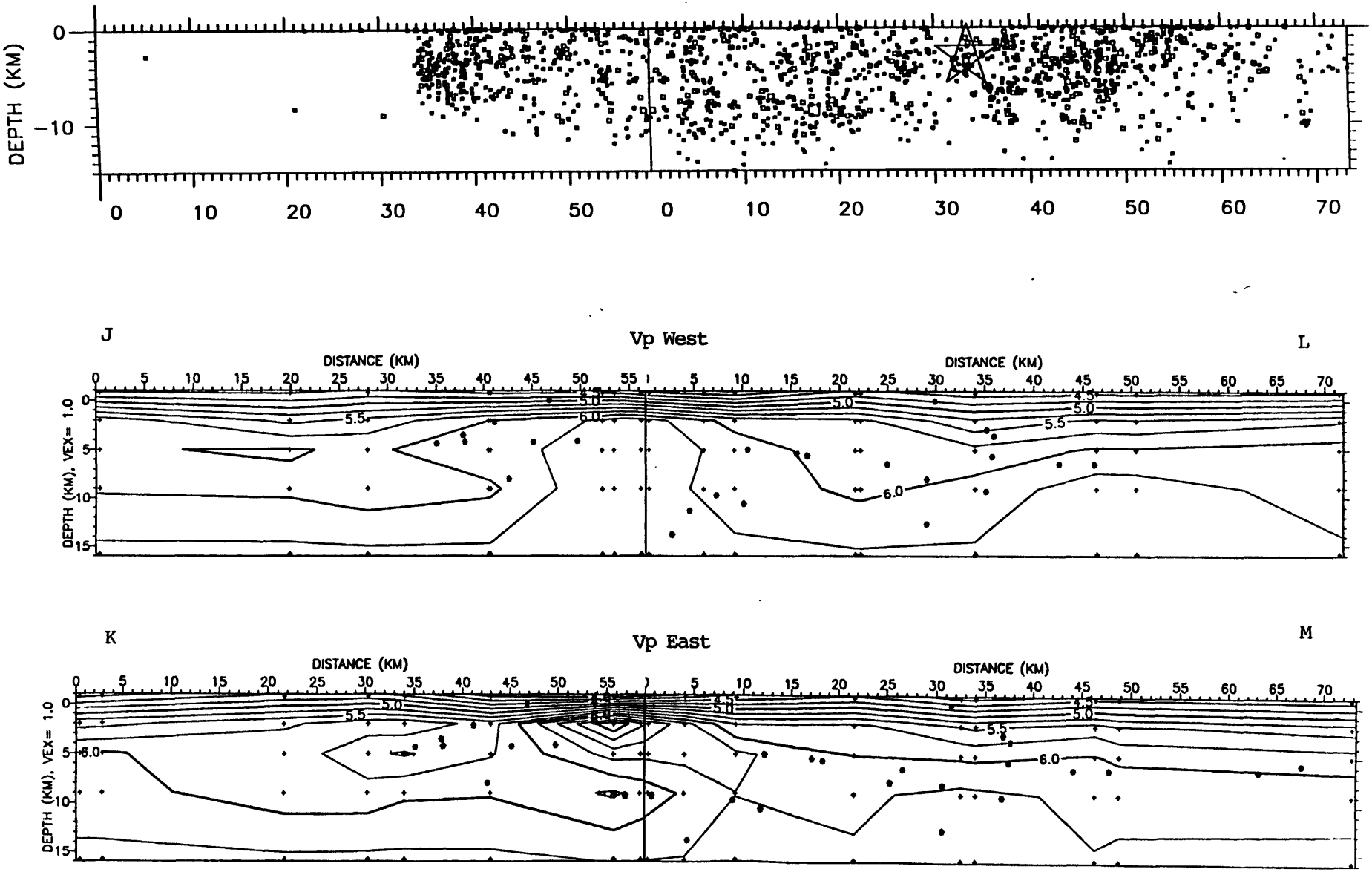

Figure 6. Top panel shows a cross section of aftershock locations along the Landers fault. Bottom two panels show P-wave velocities (Vp) interpolated onto cross-sections on either side and approximately parallel to the Landers rupture. Velocities are km/sec with 0.25 km/sec contours.

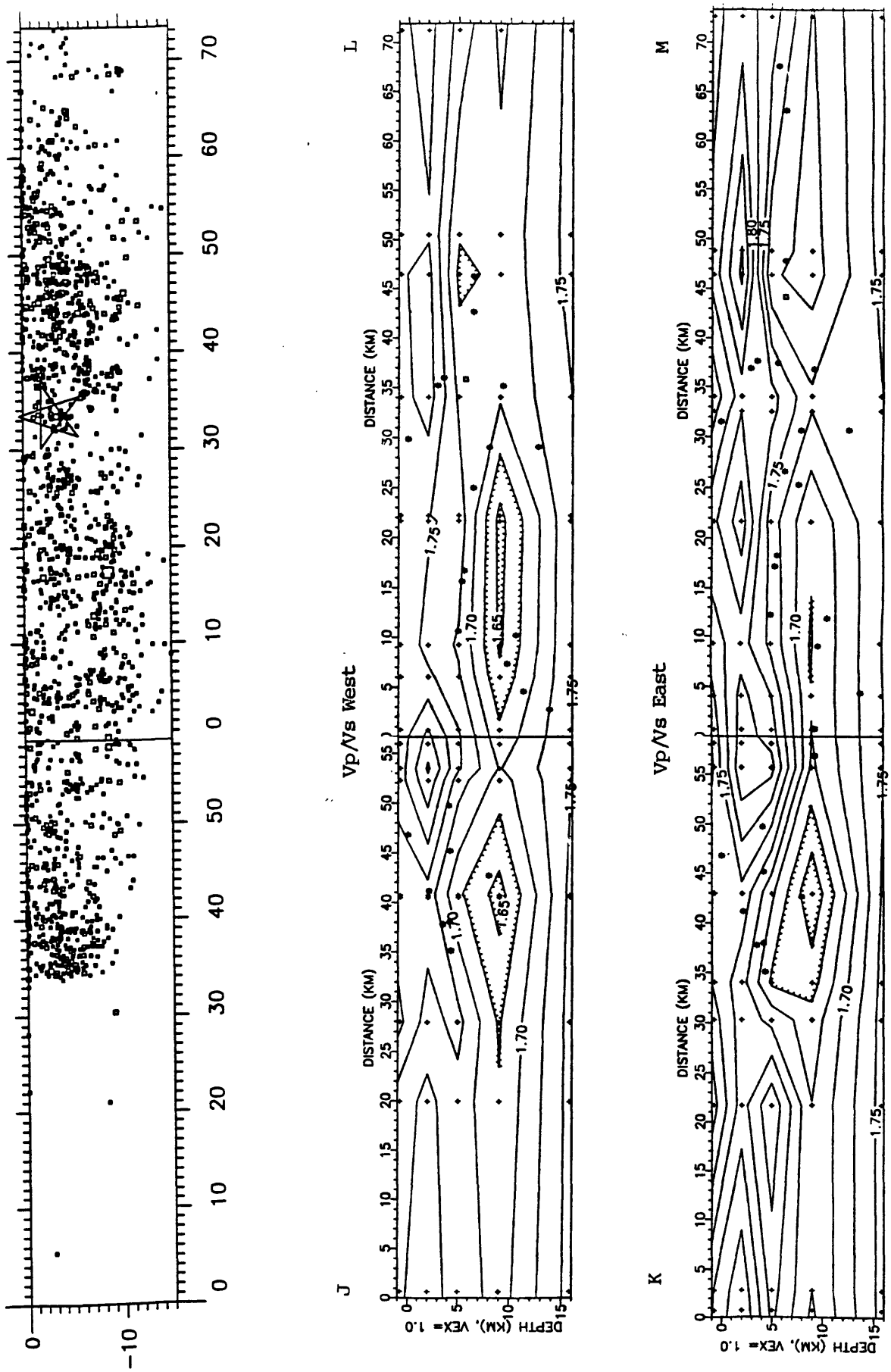

Figure 7. Top panel shows a cross section of aftershock locations along the fault. Bottom two panels show P- to S-wave velocity ratios (Vp/Vs) interpolated onto cross-sections on either side and oriented approximately parallel to the Landers rupture. Contour interval is 0.025.

the northeast. Further northwest along the Camp Rock segment, the character of the velocity image changes greatly, with the region near the fault zone defined by low velocities (Figure 5, sections B and C). Thus, 20 km northwest of the high-velocity body, the volume between the Camp Rock segment and the Calico fault is characterized by low velocities and appears to have graben-like features. The seismicity does not extend through this low-velocity region. The region near Barstow (Figure 5, section A) shows a more uniform velocity, but has lower velocities at shallow depths above the seismically active zone. This section did not rupture during the Landers earthquake (Sieh et al., 1993). Similar high- and low-velocity regions along the faults zone were also seen in a study by Zhao and Kanamori. (1993) using only the SCSN data, however the locations of these features relative to the fault are likely more accurate with the additional portable stations used in this study.

The along-fault velocity cross-sections are shown in Figure 6 also show appreciable velocity variations. The region of maximum slip for the mainshock, as determined by Wald and Heaton (1994), is located along the Emerson fault segment at the bend in the cross-sections. This corresponds to the location of the high-velocity body, where there is high-velocity on both sides of the fault, and is the area of greatest complexity in the velocity image of the fault. Along the northern part of the Camp Rock segment the crustal velocities are relatively low. The rupture did not extend into this region suggesting some change in material property that tended to inhibit propagation of the earthquake. The southern end of the fault rupture also tends to have lower crustal velocities. This relationship between the material properties and fault slip is similar to results from the Parkfield segment of the San Andreas fault (Michael and Eberhart-Phillips, 1991).

The inversion results for the Vp/Vs values are shown in Figure 7. Most of the values are in the range of 1.65 to 1.75 with values that tend to be higher for shallow portions of the crust at depths less than 5 km. Also, there appear to be higher Vp/Vs

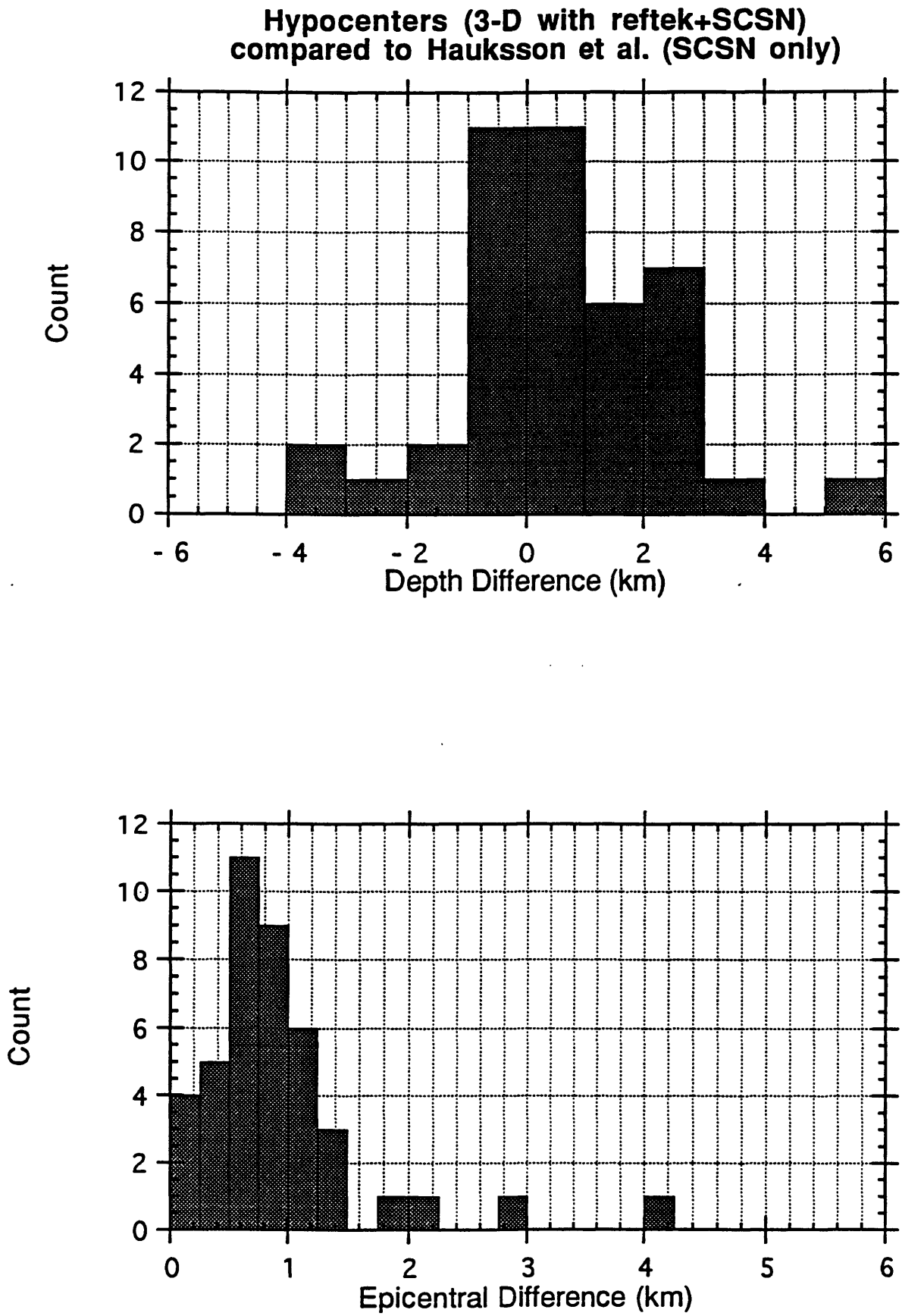

Figure 8. Depth (top) and horizontal (bottom) differences of hypocenters located with the three-dimensional model dervied in this study, compared with hypocenters located with the one-dimensional model by Hauksson et al. (1993).

Homestead Valley and Emerson segments.

HYPOCENTERS

In the process of the velocity inversion, the earthquakes used in this study were relocated. Figure 8 compares our hypocenters to those obtained with a local one-dimensional model by Hauksson et al. (1993). The addition of stations in the aftershock zone greatly effects the depth determinations, but has only minor effect on the epicenters. Generally, our hypocenters are deeper than those of Hauksson et al. (1993). With the dense distribution of portable stations along the fault during this experiment, the depths determined in our study are probably more reliable. Assuming our data give accurate depth estimates, Figure 8 is an indication of the depth uncertainties associated with the SCSN locations.

The mainshock was relocated using our velocity model and determined to be 34^{o} 12.16' N (±0.27 km), 116^{o} 26.17' W (± 0.22 km) at a depth of 3.0 km (±1.0 km).

CONCLUSIONS

The calibration experiment that was conducted along the Landers fault rupture has enabled us to image the P-wave velocity structure in the local region of a large earthquake and to determine depths of earthquakes more accurately. We found significant variations of velocity along the fault which may reflect material properties that are important in controlling the dynamics of the rupture propagation. The three-dimensional velocity inversions also provided information about the Vp/Vs variations, and showed higher Poisson's ratio at shallower (< 5 km) depths.

ACKNOWLEDGEMENTS

R. Catchings and L. Hwang assisted in leading the experiment. S. Michnick provided us with on-site knowledge of Reftek instruments. This experiment was carried

out at very short notice and many people helped in the deployment from USGS Pasadena, USGS Menlo Park, California Institute of Technology, and University of Southern California. A. Martin shared his knowledge of both instrumentation and Yucca Valley, and later provided many useful programs for extracting data from the continuous *seg-y* data. B. Julian provided his EPICK program and answered many questions about *ah* files. R. Catchings provided helpful comments on this report.

REFERENCES

Eberhart-Phillips, D., Local earthquake tomography: earthquake source regions, in *Seismic Tomography: Theory and Practice,* edited by H. M. Iyer and K. Hirahara, Chapman and Hall, London, 613-643, 1993.

Eberhart-Phillips, D., and A. J. Michael, Three-dimensional velocity structure, seismicity, and fault structure in the Parkfield region, central California, *J. Geophys. Res., 98,* 15,737-15,758, 1993.

Hauksson, E, L.M. Jones, K. Hutton, and D. Eberhart-Phillips, The 1992 Landers earthquake sequence: Seismological Observations, *J. Geophys. Res.,* 98, 19,835-19,858. 1993.

Li, Y.-G., K. Aki, D. Adams, A. Hasemi, and W.H.K. Lee, Seismic guided waves trapped in the fault zone of the Landers, California, earthquake of 1992, *J. Geophys. Res. (in press),* 1994.

Michael, A. J., and D. Eberhart-Phillips, Relations among fault behavior, subsurface geology, and three-dimensional velocity models, Relations among fault behavior, subsurface geology, and three-dimensional velocity models, *Science, 253,* 651-654, 1991.

Sieh, K., L. Jones, E. Hauksson, K. Hudnut, D. Eberhart-Phillips, T. Heaton, S. Hough, K. Hutton, H. Kanamori, A. Lilje, S. Lindvall, S. F. McGill, J. Mori, C. Rubin, J. A. Spotila, J. Stock, H.K. Thio, J. Treiman, B. Wernicke, J. Zachariasen, Near-field investigations of the Landers earthquake sequence, April to July, 1992, *Science, 260,* 171-176, 1993.

Thurber, C. H., Earthquake locations and three-dimensional crustal structure in the Coyote Lake area, central California, *J. Geophys. Res., 88,* 8226-8236, 1983.

Thurber, C. H., Local earthquake tomography: Velocities and Vp/Vs - theory, in *Seismic Tomography: Theory and Practice,* edited by H. M. Iyer and K. Hirahara, Chapman and Hall, London, 1993.

Wald, D.J. and T. H. Heaton, Spatial and temporal slip distribution during the 1992 Landers, California earthquake, *Bull. Seismol. Soc. Am. (in press),* 1994.

Zhou, D. and H. Kanamori, The 1992 Landers earthquake sequence: Earthquake occurence and structural heterogeneities, *Geophys. Res. Lett., 20,* 1083-1086, 1993.

Station	Latitude (Deg.	Min.)	Longitude (Deg.	Min.)	Elevation (m)
LB3	33	48.12	116	18.03	56
L01	33	53.10	116	19.34	351
L02	33	54.82	116	19.42	528
L03	34	0.57	116	18.32	1585
L04	34	2.97	116	18.97	1504
L05	34	4.25	116	20.62	1398
L06	34	5.62	116	22.14	1239
L07	34	7.26	116	22.11	1088
L08	34	8.63	116	23.16	1068
L09	34	9.66	116	23.70	1150
L10	34	10.72	116	24.23	1176
L11	34	11.81	116	24.76	1167
L12	34	12.89	116	25.13	1148
L14	34	15.06	116	26.05	1120
LU3	34	16.27	116	26.38	1105
L15	34	16.15	116	26.32	1104
L16	34	17.21	116	26.74	1084
L18	34	19.38	116	27.63	1046
L19	34	20.36	116	28.39	1044
L20	34	21.44	116	28.84	989
L21	34	22.43	116	29.57	933
L22	34	23.60	116	29.65	865
L23	34	24.94	116	30.73	846
L24	34	25.84	116	30.29	859
L25	34	27.06	116	30.30	912
L26	34	27.72	116	32.10	933
L27	34	29.06	116	31.67	1035
L28	34	30.85	116	29.89	925
L29	34	33.27	116	30.45	896
L40	34	40.68	116	43.28	1309
L39	34	40.18	116	41.84	1337
L42	34	42.35	116	45.76	1257
L43	34	42.87	116	46.51	1260
L44	34	43.52	116	47.65	1293
L45	34	44.11	116	48.97	1296
L46	34	45.58	116	49.03	1239
L47	34	46.41	116	49.96	1150
L48	34	47.55	116	50.49	1032
L49	34	48.92	116	50.72	896
LA1	34	45.89	116	22.66	709
LA2	34	38.51	116	9.05	681

Table 2. Station coordinates of portable instrument sites deployed for the calibration experiment.

Station	DAS#	Recorded Offset(s)	Recorded Drift	Lab Test Drift	Estimated Offset(s)	Calculated Sta. Corr.
LB3	6049	0.805	3.526e-07			
L01	6055	15.411	-1.441e-07			
L02	6093	-1.442		-4.6e-08		
L03	6023	-0.592	-3.934e-07			
L04	6083	8.873	-4.745e-08			
L05	6108	-1.378	-2.589e-06			
L06	6117	0.522		1.4e-07		
L07	6127	0.395	4.967e-11			
L08	6037	0.851	-1.987e-09			
L09	6044	0.273	-3.379e-06			
L10	6048				-0.800	0.928
L11	6118	-11.634	-2.409e-07			
L12	6111	0.205	1.409e-07			
L14	6115	-3.029	4.680e-07			
LU3	6041				0	0.257
L15	6100	20.149	-4.275e-07			
L16	6086	7.012	-1.589e-09			
L18	6038	-1.782	-1.433e-07			
L19	6024			3.5e-08	79.525	-0.036
L20	6084	-12.864	-1.589e-09			
L21	6088			9.5e-07	-56.335	0.027
L22	6120	1.314	-9.272e-10			
L23	6056	0.564		-3.1e-07		
L24	6114	0.496		2.2e-07		
L25					102.79	-0.005
L26	6110				-63.545	0.136
L27	6129	0.280		3.2e-07		
L28	6021			2.7e-07	0	1.144
L29	6116	-0.059	-1.656e-11			
L39	6119			1.3e-07	-0.69	0.482
L40	6098	0.180				
L42	6099	9.504	-1.700e-06			
L43	6123	0.838	-1.592e-06			
L44	6091			7.3e-08	17.6	0.581
L45	6087	4.591	-2.137e-06			
L46	6092	-0.587	-1.526e-06			
L47	6080	8.794	-1.685e-06			
L48	6052				0.44	0.710
L49	6121			3.8e-07	16.1	0.408
LA1	6065	8.193	-4.8e-10			
LA2	6097	8.660				

Table 3. Clock correction parameters.

92198213435.ah	92198215814.ah	92198222510.ah	92198222812.ah
92198223419.ah	92198223559.ah	92198224425.ah	92198224441.ah
92198230337.ah	92198231252.ah	92198232218.ah	92198232359.ah
92198232504.ah	92198232604.ah	92198233554.ah	92198234421.ah
92198234808.ah	92199000604.ah	92199001828.ah	92199003115.ah
92199003407.ah	92199004409.ah	92199004737.ah	92199004828.ah
92199004844.ah	92199004942.ah	92199005148.ah	92199005233.ah
92199005840.ah	92199010206.ah	92199010914.ah	92199010938.ah
92199011403.ah	92199012134.ah	92199012218.ah	92199012444.ah
92199013422.ah	92199014308.ah	92199014457.ah	92199014630.ah
92199014817.ah	92199015446.ah	92199015524.ah	92199020023.ah
92199020154.ah	92199020222.ah	92199020433.ah	92199020529.ah
92199020944.ah	92199021107.ah	92199021405.ah	92199021902.ah
92199022042.ah	92199022139.ah	92199022627.ah	92199023322.ah
92199023630.ah	92199023714.ah	92199023751.ah	92199024343.ah
92199024431.ah	92199024703.ah	92199024824.ah	92199025030.ah
92199025228.ah	92199025707.ah	92199025935.ah	92199030009.ah
92199030047.ah	92199030449.ah	92199030508.ah	92199030912.ah
92199031143.ah	92199031223.ah	92199031232.ah	92199031928.ah
92199032114.ah	92199032301.ah	92199032618.ah	92199032754.ah
92199033120.ah	92199033141.ah	92199033217.ah	92199033256.ah
92199033413.ah	92199033430.ah	92199033619.ah	92199034433.ah
92199034809.ah	92199034841.ah	92199035415.ah	92199035542.ah
92199035746.ah	92199035757.ah	92199040000.ah	92199040222.ah
92199040302.ah	92199040606.ah	92199040734.ah	92199040944.ah
92199040952.ah	92199041223.ah	92199041229.ah	92199041505.ah
92199041627.ah	92199041643.ah	92199041756.ah	92199041914.ah
92199042029.ah	92199042120.ah	92199042226.ah	92199042621.ah
92199042701.ah	92199042908.ah	92199042952.ah	92199043230.ah
92199043549.ah	92199043746.ah	92199043916.ah	92199044124.ah
92199044319.ah	92199044630.ah	92199044648.ah	92199044704.ah
92199044802.ah	92199044814.ah	92199045136.ah	92199045207.ah
92199045855.ah	92199045919.ah	92199050709.ah	92199051150.ah
92199051244.ah	92199051422.ah	92199051625.ah	92199051630.ah
92199051641.ah	92199052010.ah	92199052140.ah	92199053222.ah
92199053238.ah	92199053325.ah	92199053634.ah	92199053805.ah
92199054019.ah	92199054216.ah	92199054629.ah	92199055359.ah
92199055446.ah	92199055518.ah	92199055621.ah	92199055951.ah
92199060049.ah	92199060142.ah	92199060253.ah	92199060343.ah
92199060348.ah	92199060634.ah	92199060830.ah	92199060922.ah
92199061422.ah	92199061635.ah	92199061739.ah	92199062919.ah

Table 4. Earthquake event files recorded during calibration experiment

92199063202.ah	92199063356.ah	92199063628.ah	92199063711.ah
92199063715.ah	92199064230.ah	92199064253.ah	92199064344.ah
92199064900.ah	92199064949.ah	92199065005.ah	92199065142.ah
92199065224.ah	92199065319.ah	92199065402.ah	92199065914.ah
92199070103.ah	92199070154.ah	92199070220.ah	92199070726.ah
92199070837.ah	92199070904.ah	92199071001.ah	92199071301.ah
92199071416.ah	92199071421.ah	92199071447.ah	92199071607.ah
92199071629.ah	92199071840.ah	92199071856.ah	92199071944.ah
92199072139.ah	92199072159.ah	92199072306.ah	92199072442.ah
92199072859.ah	92199073337.ah	92199073536.ah	92199074824.ah
92199075258.ah	92199075350.ah	92199075452.ah	92199075749.ah
92199080326.ah	92199080704.ah	92199080726.ah	92199080900.ah
92199081603.ah	92199081650.ah	92199082242.ah	92199082329.ah
92199082413.ah	92199082759.ah	92199082834.ah	92199082908.ah
92199083747.ah	92199083836.ah	92199084102.ah	92199084154.ah
92199084317.ah	92199084549.ah	92199084906.ah	92199085202.ah
92199085341.ah	92199085617.ah	92199085633.ah	92199085722.ah
92199090059.ah	92199090549.ah	92199091017.ah	92199091128.ah
92199091711.ah	92199091714.ah	92199092047.ah	92199092217.ah
92199092306.ah	92199092310.ah	92199092745.ah	92199092943.ah
92199092959.ah	92199093203.ah	92199094509.ah	92199094623.ah
92199094738.ah	92199094915.ah	92199095358.ah	92199095753.ah
92199095757.ah	92199095855.ah	92199100212.ah	92199100620.ah
92199101644.ah	92199101751.ah	92199101913.ah	92199102301.ah
92199102345.ah	92199102424.ah	92199102429.ah	92199102554.ah
92199102640.ah	92199102807.ah	92199102905.ah	92199103128.ah
92199103404.ah	92199104008.ah	92199104112.ah	92199104906.ah
92199105011.ah	92199105207.ah	92199105452.ah	92199105545.ah
92199105603.ah	92199105931.ah	92199105936.ah	92199110224.ah
92199110313.ah	92199110450.ah	92199110900.ah	92199111307.ah
92199111354.ah	92199111558.ah	92199111618.ah	92199111724.ah
92199112808.ah	92199113044.ah	92199113206.ah	92199113509.ah
92199113818.ah	92199114202.ah	92199114246.ah	92199114356.ah
92199114514.ah	92199114600.ah	92199114950.ah	92199115057.ah
92199115134.ah	92199115223.ah	92199115349.ah	92199115528.ah
92199115636.ah	92199115817.ah	92199115824.ah	92199120307.ah
92199120427.ah	92199120941.ah	92199121013.ah	92199121051.ah
92199121238.ah	92199121330.ah	92199121443.ah	92199121654.ah
92199121752.ah	92199122124.ah	92199122127.ah	92199122232.ah
92199123058.ah	92199123231.ah	92199123759.ah	92199124427.ah
92199124510.ah	92199124612.ah	92199124741.ah	92199124747.ah
92199124935.ah	92199125112.ah	92199125321.ah	92199125337.ah
92199125615.ah	92199125702.ah	92199130030.ah	92199130354.ah

Table 4 (cont). Earthquake event files recorded during calibration experiment

92199130451.ah	92199131448.ah	92199131753.ah	92199131919.ah
92199132159.ah	92199132215.ah	92199132243.ah	92199132434.ah
92199132625.ah	92199132750.ah	92199132846.ah	92199132852.ah
92199132935.ah	92199133023.ah	92199133228.ah	92199133351.ah
92199133426.ah	92199133757.ah	92199134241.ah	92199134308.ah
92199134448.ah	92199134451.ah	92199134703.ah	92199134723.ah
92199134931.ah	92199135118.ah	92199135207.ah	92199135515.ah
92199135616.ah	92199140002.ah	92199140117.ah	92199140721.ah
92199140937.ah	92199141117.ah	92199141134.ah	92199141243.ah
92199141246.ah	92199141429.ah	92199141811.ah	92199142006.ah
92199142117.ah	92199142352.ah	92199142417.ah	92199142630.ah
92199142844.ah	92199142938.ah	92199143115.ah	92199143131.ah
92199143300.ah	92199143657.ah	92199143739.ah	92199143915.ah
92199143938.ah	92199144027.ah	92199144143.ah	92199144650.ah
92199144721.ah	92199145136.ah	92199145518.ah	92199145758.ah
92199150202.ah	92199150547.ah	92199150757.ah	92199151034.ah
92199151114.ah	92199151130.ah	92199151309.ah	92199151357.ah
92199151757.ah	92199152152.ah	92199152220.ah	92199152244.ah
92199152321.ah	92199152705.ah	92199152755.ah	92199152944.ah
92199152946.ah	92199153044.ah	92199153100.ah	92199153405.ah
92199153704.ah	92199153752.ah	92199153922.ah	92199154106.ah
92199154224.ah	92199154240.ah	92199154416.ah	92199154534.ah
92199154800.ah	92199154918.ah	92199155636.ah	92199155709.ah
92199155935.ah	92199160012.ah	92199160019.ah	92199160515.ah
92199160940.ah	92199160943.ah	92199161459.ah	92199161515.ah
92199162118.ah	92199162211.ah	92199162338.ah	92199162343.ah
92199162715.ah	92199162802.ah	92199163058.ah	92199163244.ah
92199163722.ah	92199163905.ah	92199164122.ah	92199164231.ah
92199164247.ah	92199164636.ah	92199165022.ah	92199165044.ah
92199165100.ah	92199165420.ah	92199170312.ah	92199170440.ah
92199170444.ah	92199170531.ah	92199170650.ah	92199170736.ah
92199170857.ah	92199171143.ah	92199171351.ah	92199171616.ah
92199171711.ah	92199171733.ah	92199171828.ah	92199172002.ah
92199172156.ah	92199172345.ah	92199172401.ah	92199172833.ah
92199173653.ah	92199174112.ah	92199174214.ah	92199174327.ah
92199174624.ah	92199174640.ah	92199174821.ah	92199175019.ah
92199180002.ah	92199180052.ah	92199180552.ah	92199180638.ah
92199182157.ah	92199182159.ah	92199182619.ah	92199182709.ah
92199183209.ah	92199183248.ah	92199183318.ah	92199183501.ah
92199183650.ah	92199184034.ah	92199184629.ah	92199184737.ah

Table 4 (cont). Earthquake event files recorded during calibration experiment